Nature of the Mn Centers in Photosystem II. Modeling and Behavior of the $g = 4$ Resonances and Related Signals

Karin A. Åhrling,[†,‡] Paul J. Smith,[†,‡] and Ronald J. Pace*[,†]

Contribution from the Department of Chemistry, Australian National University, Canberra 0200 Australia, and Cooperative Research Center for Plant Science, Canberra, 2601, Australia

Received April 29, 1998. Revised Manuscript Received October 13, 1998

Abstract: The two forms of the $g \approx 4.1$ signal recently identified in photosystem II (Smith, P. J.; Pace, R. J. *Biochim. Biophys. Acta* **1996**, *1275*, 213) have been simulated at several frequencies as near-axial spin $^3/_2$ centers. In both cases, an explicit spin coupling model is assumed, involving two magnetically isolated Mn pairs, one for each signal type. For that pair assumed to give rise to the spin $^1/_2$ multiline signal as the ground state, the modeling of the first-excited-state 4.1 signal gives estimates of the fine structure parameters for the individual Mn centers and the exchange coupling constant for the pair. The fine structure terms suggest that one Mn ion is a conventional Mn^{III} ion in a highly axially distorted environment. The other Mn center, which is formally spin $^3/_2$, is unlikely to be a conventional Mn^{IV} ion, but rather a Mn^{III}−radical ligand pair, strongly antiferromagnetically coupled to give a net spin $^3/_2$ state. The coupling between this Mn−radical center and the other Mn^{III} is weak ($J = -2.3$ cm^{-1}) in the absence of alcohol in the buffer medium, as determined earlier (Smith and Pace). The model is shown to be quantitatively consistent with the behavior of other signals proposed to arise from this coupled dimer. Comparison of our own data with those of others (Haddy, A.; et al. *Biochim. Biophys. Acta* **1992**, *1099*, 25−34) on one-dimensionally ordered photosystem II samples shows a generally consistent orientation of the molecular axis system for the dimer in the membrane plane. The second 4.1 signal, which exhibits ground-state behavior, may be simulated at X- and Q-band frequencies as an isolated system with $D = +1.1$ cm^{-1} and $E/D = 0.037$. The spin center is suggested to arise from a radical-bridged Mn homodimer, and the modeling parameters have been interpreted within this framework. The resulting proposal, involving two isolated dimers for the Mn organization within the oxygen evolving center, is critically examined in the light of recent work from other groups.

Introduction

The catalytic water oxidation site in photosystem II (PSII) of higher plants, bacteria, and algae contains four Mn ions in an as-yet undetermined geometry.[1] This site, together with several protein-associated cofactors, forms the oxygen evolving center (OEC). The oxygen formation reaction proceeds through five intermediates of the OEC (S-states), labeled S_0-S_4, where the subscript refers to the number of positive redox equivalents stored. Each S-state forms progressively by single electron transfer from the OEC components to the photo-oxidized reaction center, $P680^+$. Mn extended X-ray absorption fine structure (EXAFS) studies by several groups[2−4] have established that the dominant structural organization of the Mn is two μ-oxo-bridged dimers, with a Mn−Mn separation in each of ∼2.7 Å.

One S-state, S_2, has long been known to exhibit Mn-derived EPR signals at low temperature.[1] Two characteristic signals have been reported: a Mn hyperfine structured signal centered at $g = 2.0$ (the multiline), known to arise from a net spin $^1/_2$ ground-state system involving at least a Mn pair, and a broad resonance around $g = 4$ (the 4.1 signal). The latter is a signal of 30−35-mT width[5−7] and is known to involve at least a Mn pair.[8,9] There has been some debate as to how the signal appears: it has been considered a ground $S = ^3/_2$ state[7] and also shown to be a first excited $S = ^3/_2$ state of the ground $S = ^1/_2$ multiline state.[10] Recently, Smith and Pace have shown[10−12] that there are two forms of the 4.1 signal. One is generated by illumination at 130 K with the PSII preparation in a buffer containing 30% ethylene glycol, and is shown by temperature dependence studies to be a ground state. It was suggested to arise from a bridged dimer of Mn^{III}, in a net $S = 1$ state, coupled to a radical. The total interaction is then $S = ^3/_2$. The other form of the 4.1 signal is confirmed by temperature dependence studies to be the first excited, $S = ^3/_2$ state of the $S = ^1/_2$ ground-state multiline signal, proposed to arise from a $Mn^{III}-Mn^{IV}$ di-μ-oxo-bridged dimer.

† Australian National University.
‡ Cooperative Research Center for Plant Science.

(1) Debus, R. J. *Biochim. Biophys. Acta* **1992**, *1102*, 269−352.
(2) Yachandra, V. K.; Guiles, R. D.; McDermott, A. E.; Cole, J. L.; Britt, R. D.; Dexheimer, S. L.; Sauer, K.; Klein, M. P. *Biochemistry* **1987**, *26*, 5974−5981.
(3) Penner-Hahn, J. E.; Fronko, R. M.; Pecoraro, V. L.; Yocum, C. F.; Betts, S. D.; Bowlby, N. R. *J. Am. Chem. Soc.* **1990**, *112*, 2549−2557.
(4) MacLachlan, D. J.; Hallahan, B. J.; Ruffle, S. V.; Nugent, J. H. A.; Evans, M. C. W.; Strange, R. W.; Hasnain, S. S. *Biochem. J.* **1992**, *285*, 569−576.
(5) Casey, J. L.; Sauer, K. *Biochim. Biophys. Acta* **1984**, *767*, 21−28.
(6) Zimmerman, J.; Rutherford, A. W. *Biochim. Biophys. Acta* **1984**, *767*, 160−167.
(7) Hansson, O.; Aasa, R.; Vänngård, T. *Biophys. J.* **1987**, *51*, 825−832.
(8) Kim, D. H.; Britt, R. D.; Klein, M. P.; Sauer, K. *J. Am. Chem. Soc.* **1990**, *112*, 9389−9391.
(9) Kim, D. H.; Britt, R. D.; Klein, M. P.; Sauer, K. *Biochemistry* **1992**, *31*, 541−547.
(10) Smith, P. J.; Åhrling, K. A.; Pace, R. J. *J. Chem. Soc., Faraday Trans.* **1993**, *89*, 2863−2868.
(11) Smith, P. J.; Pace, R. J. *Biochim. Biophys. Acta* **1996**, *1275*, 213−220.
(12) Smith, P. J.; Pace, R. J. *Appl. Magn. Reson.* **1996**, *11*, 443−460.

10.1021/ja981471c CCC: $15.00
Published on Web 12/04/1998

In addition, a Mn hyperfine structured signal at $g \approx 6$, with a temperature dependence consistent with it arising from the next higher state ($S = {}^5/_2$) in the manifold, was also seen. These signals are cogenerated by illumination at 200 K. The presence of small monoalcohols suppresses this form of the 4.1 signal (ref 12 and references noted therein). The ground-state form of the signal, however, requires the presence of ethylene glycol (30% v/v in final buffer) or glycerol (50% v/v), which is the regime in which Casey and Sauer first saw the signal.[5]

Haddy et al.[13] have simulated the 4.1 signal at S-, X-, and P-band (15 GHz) and suggested it to arise from a near-rhombic $S = {}^5/_2$ state. Astashkin et al.[14] also concluded, from a pulsed EPR study, that the 4.1 signal arises from an $S = {}^5/_2$ state. However, this analysis and conclusion have been questioned.[11] Detailed examination of the temperature dependences of both types of 4.1 signal, combined with their shapes at X- and Q-band, makes it very unlikely that either signal arises from near-rhombic spin ${}^5/_2$ states.[11] A spin ${}^3/_2$ assignment for the 4.1 signal(s) has also been suggested by Kusunoki et al.[15]

We have proposed that the Mn in the OEC are arranged as two exchange-coupled pairs (Mn−Mn separation 2.7 Å) which are themselves sufficiently separated not to directly magnetically interact.[11] A strong element of the argument is the demonstrated existence of two forms of 4.1 signal, each associated with a separate Mn dimer. This is supported by the observation, originally by Dexheimer and Klein,[16] that an even spin parallel polarization signal ($g \approx 5$) observed in the S_1 state of PSII could coexist with one type of the formal S_2-state signal (the ground-state 4.1), but not the other type (multiline). Kawamori et al.[17] have confirmed this and shown that the S_1 signal arises from a weakly excited state (probably spin 1) and is abolished by alcohol (2% MeOH) in the buffer medium. This argues strongly for a "separate centers" assignment of the species responsible for the multiline (and parallel polarization) signal and the ground-state 4.1 signal.

In this study, we develop detailed magnetic models for the two Mn dimer centers from simulation of the two 4.1 signal types at various frequencies (S-, X-, P-, Q-bands), as well as the temperature dependences of these and related signals. We consider data on oriented and powder pattern systems from ourselves and other groups.[13] The spin ${}^3/_2$ signals provide sensitive information on the single-ion fine structure terms of the various Mn centers, which complement our earlier multifrequency studies[18] on the hyperfine modeling of the Mn dimer responsible for the S_2-state multiline signal.

Method

(a) Experimental Details. Spectra for oriented and unoriented samples at X- and Q-band for the two types of 4.1 signal species were taken from previously published results of this group.[10,11] The sample orientation technique was derived from that of Rutherford.[19]

(b) Theory. The spin Hamiltonian for an $S = {}^3/_2$ system has the form

$$H = \beta \cdot \mathbf{H_o} \cdot \boldsymbol{g} \cdot \mathbf{S} + \mathbf{S} \cdot \boldsymbol{D} \cdot \mathbf{S} + \sum_i (\mathbf{S} \cdot \boldsymbol{A}_i \cdot \mathbf{I}_i + \mathbf{I}_i \cdot \boldsymbol{Q}_i \cdot \mathbf{I}_i) \quad (1)$$

$\boldsymbol{D}$ is the zero field splitting (ZFS) tensor. The hyperfine interactions (the expression in parentheses) contain contributions from the anisotropic Fermi contact plus dipolar terms ($\boldsymbol{A}$) and nuclear quadrupole interaction ($\boldsymbol{Q}$). Here, their effect is calculated for each atom involved, as a perturbation on the main transitions induced by the ZFS terms. Usually, the zero field Hamiltonian, H_D, is expressed in the principal axis form:

$$H_D = D(S_z^2 - {}^1/_3 S^2) + E(S_x^2 + S_y^2) \quad (2)$$

where $D = {}^3/_2 D_{zz}$ and $E = (D_{xx} - D_{yy})/2$.

In an exchange-coupled cluster, in which the exchange term(s) dominate, S is the net spin of the system in one of the eigenstates of the spin coupled manifold. The $\boldsymbol{g}$, $\boldsymbol{D}$, and $\boldsymbol{A}$ tensors in eq 1 are then effective terms, related to the "projection" of the corresponding individual single-ion parameters onto the net spin state. These projections are readily determined, for systems of sufficient simplicity or symmetry, when the exchange interactions are large compared to the individual single-ion terms (usually the fine structure terms).[20] In this strong exchange limit, the projections are obtained from first-order perturbation theory. In the intermediate exchange region (exchange interaction less than 1 order of magnitude larger than other terms), the exchange interaction still dominates and establishes a manifold of net spin states, but the projection terms are now sensitive to the magnitudes of the exchange interactions.[20] In this situation there are two options: (i) solve the system exactly using products of the individual center spin functions as basis, or (ii) solve within the exchange-coupled spin manifold formalism, but use higher (second)-order perturbation theory to evaluate the effective spin Hamiltonian terms. This has the virtue of being computationally much simpler and more analytically transparent. We employ this procedure for the analysis of those signals arising from the weakly (in the absence of alcohol) exchange-coupled Mn pair responsible for the multiline and related signals in our model. In this system, the exchange interaction is 2−3 times larger than the individual Mn ion fine structure terms, placing it directly in the intermediate exchange region. For the other Mn pair, which forms part of a postulated three-spin-center system,[12] the data at present do not compel a treatment beyond the assumption of the strong exchange limit, which is then used here.

(c) Simulations. In both cases, modeling of the relevant 4.1 signal in oriented or powder pattern samples is in terms of a net spin ${}^3/_2$ center (eqs 1 and 2), with appropriate effective spin Hamiltonian parameters. All possible transitions are included by the matrix diagonalization method used here. The simulation program for the two forms of the 4.1 signal draws on the method given in ref 18 for the multiline simulation, with a field position resolution of 0.1 mT. Transition probabilities are computed from

$$|\langle m_\uparrow | \mathbf{H}_1 \cdot \boldsymbol{g} \cdot \mathbf{S} | m_\downarrow \rangle|^2 = H_1^2 [\langle m_\uparrow | \cos\gamma (g_{xx} S_x + g_{xy} S_y + g_{xz} S_z) + \sin\gamma (g_{yx} S_x + g_{yy} S_y + g_{yz} S_z) | m_\downarrow \rangle]^2 \quad (3)$$

Here, $m_\uparrow$ and $m_\downarrow$ stand for the spin-up and spin-down eigenvectors, as generated by the matrix diagonalization of the main Hamiltonian expression. γ is the Euler angle defining the H_1 field orientation relative to the molecular axis.[18] This is averaged by integration around γ for unoriented samples.

(d) Hyperfine Interaction. For the excited-state $g = 4.1$ case, the magnitudes of the hyperfine interactions in the $Mn^{III}-Mn^{IV}$ dimer are known from the multiline simulation.[18] The hyperfine interaction (expression in parentheses in eq 1) has therefore been included in the calculation. For Mn^{III}, as it is quasi-axial, the interaction has been included as a perturbation term for the hyperfine interaction only. For Mn^{IV}, because of the unique low-symmetry interactions proposed, the energy terms due to the hyperfine and quadrupole interactions are

(13) Haddy, A.; Dunham, W. R.; Sands, R. H.; Aasa, R. *Biochim. Biophys. Acta* **1992**, *1099*, 25−34.
(14) Astashkin, A. V.; Kodera, Y.; Kawamori, A. *J. Magn. Reson.* **1994**, *B105*, 113−119.
(15) Kusunoki, M.; Ono, T.; Suzuki, M.; Noguchi, T.; Uehara, A.; Matsushita, T.; Oyanagi, H.; and Inoue, Y. *Research in Photosynthesis*, Vol. II.; Murata, N., Ed.; Kluwer Academic Publishers: Dordrecht, 1992; pp 293−296.
(16) Dexheimer, S. L.; Klein, M. P. *J. Am. Chem. Soc.* **1992**, *114*, 2821−2826.
(17) Yamauchi, T.; Mino, H.; Matsukawa, T.; Kawamori, A.; Ono, T. *Biochemistry* **1997**, *36*, 7520−7526.
(18) Åhrling, K. A.; Pace, R. J. *Biophys. J.* **1995**, *68*, 2081−2090.
(19) Rutherford, A. W. *Biochim. Biophys. Acta* **1985**, *807*, 189−201.
(20) Bencini, A.; Gatteschi, D. *Electron Paramagnetic Resonance of Exchange Coupled Systems* 1st ed.; Springer-Verlag: Berlin, 1990.

calculated by the diagonalization of two 6 × 6 matrixes. These energy terms, together with the Mn^{III} perturbation terms, modify the main transitions.

For the ground-state 4.1 simulation, the program includes only the hyperfine interactions of the two Mn^{III} as simple perturbations to the main transitions. It does not include the hyperfine interaction for the radical, as it is assumed to be small. This third spin center does, however, affect the projection operators calculated for the hyperfine interactions.

Effective hyperfine coupling coefficients are calculated from projection operators according to the method given in ref 20. For an isolated pair of $Mn^{III}-Mn^{IV}$ with a net $S = {}^3/_2$ state, they are ${}^4/_5$ for Mn^{III} and ${}^1/_5$ for Mn^{IV}. However, when $D/J \approx 1$, as is the case for the excited-state 4.1 signal,[10,11] this relationship usually breaks down,[21] and the coefficients tend to approach each other. Since we do not seek to address this underlying structure in detail here, beyond its contribution to the overall 4.1 signal shape, nor model the intrinsic line width as anything other than an isotropic Gaussian (it is probably significantly anisotropic, as has been assumed by others[13]), we have subsumed these uncertainties into the projection coefficients and allowed them to vary somewhat from the nominal strong exchange values.

In the case of the ground-state form, with three interacting spin centers, the net projection operator is ${}^1/_3$ for each in the strong coupling limit, which is assumed here.

(e) Simulation of One-Dimensionally Ordered Samples. To simulate the spectra of one-dimensionally ordered samples, two sets of rotations are performed on going from the molecular frame to the laboratory axis. One set describes the orientation of the molecular axis relative to the Mylar sheet normal (α, rotation about *z*-axis; β, rotation about *y*-axis), the other the orientation of the membrane plane normal relative to the applied magnetic field (ϕ, rotation about *z*-axis, θ, rotation about *y*-axis) (see ref 19 and description given in ref 18). A Gaussian distribution of the angle between the thylakoid membrane normal and the Mylar sheet was included, with variance of about 15°.

For one-dimensionally oriented samples, the H_1 field is always in the Mylar plane for the TE_{102} cavity geometry used here. This defines the laboratory *y*-axis. The transition probabilities are therefore calculated from

$$H_1{}^2|\langle m_\uparrow|g_{xy}S_x + g_{yy}S_y + g_{zy}S_z|m_\downarrow\rangle|^2 \qquad (4)$$

For the transition probabilities, then, the rotations α and β as above describe the orientation of the molecule relative to the membrane plane, ϕ describes the orientation of the resulting membrane *y*-axis relative to the H_1 field, and θ describes the orientation of the Mylar plane normal to the incident H_o field. ϕ varies between 0 and 2π to generate a one-dimensionally ordered powder pattern, and θ may take values between 0 and $\pi/2$.

(f) Intermediate Exchange Calculations. Previously we have suggested[10] that the 4.1 signals, assumed to be spin ${}^3/_2$ states, arise from near-axial centers, and this is confirmed by the spectral simulations below. We assume, therefore, that the individual $\boldsymbol{D}$ tensors for the weakly coupled Mn in the multiline generating dimer are themselves essentially axial and, for simplicity, parallel.[18] The total spin Hamiltonian (neglecting hyperfine interactions) then becomes

$$H_{ZF} = -2J\boldsymbol{S_1}\cdot\boldsymbol{S_2} + D_1[S_{1z}{}^2 - {}^1/_3 S_1(S_1+1)] + D_2[S_{2z}{}^2 - {}^1/_3 S_2(S_2+1)] + \beta\mathbf{H}\cdot(\boldsymbol{g_1}\cdot\mathbf{S_1} + \boldsymbol{g_2}\cdot\mathbf{S_2}) \qquad (5)$$

J is the antiferromagnetic exchange coupling constant, whose magnitude we have previously estimated to be ~2 cm^{-1} in alcohol-free PSII.[11,22] S_1 and S_2 refer to the total spins of the individual Mn centers, assumed to be $S_1 = 2$ and $S_2 = {}^3/_2$, for a $Mn^{III}-Mn^{IV}$ heterodimer. The *z*-axis for this system is the symmetry axis for the $\boldsymbol{D}$ tensors. Multifrequency simulations of the multiline state[18] in the presence of alcohol (when $J > 10$ cm^{-1}, essentially strong exchange limit)[21] have indicated that the effective $\boldsymbol{g}$ tensor for this state is nearly isotropic and close to 2.00. We assume therefore that the $\boldsymbol{g}_1$ and $\boldsymbol{g}_2$ tensors are equal and parallel, so that the Zeeman term in eq 5 becomes

$$H_{Zeeman} = \beta\mathbf{H}_o\cdot\boldsymbol{g}\cdot\mathbf{S} \qquad \mathbf{S} = \mathbf{S}_1 + \mathbf{S}_2; \quad \boldsymbol{g} = \boldsymbol{g}_1 = \boldsymbol{g}_2 \qquad (6)$$

Equations 5 and 6 are then solved to second-order perturbation theory, using as basis the spin-coupled wave functions, $|S_1,S_2, S\ M\rangle$, which are the eigenfunctions of the leading (zero order) exchange coupling term in eq 5 (Appendix 1). Within a given *S* manifold (e.g., $S = {}^3/_2$), the first-order solution corresponds to solving eq 1 in the strong exchange limit. In second order, the fine structure terms in eq 5 cause mixing of the $S = {}^3/_2$ states with those of different *S* (up to $S \pm 2$) but the same *M* values, while the Zeeman term, when of the form of eq 6, never mixes states of different *S*.

For a simple axial or near-axial $S = {}^3/_2$ system, the powder pattern spectrum is normally dominated by the $|-{}^1/_2\rangle$ to $|+{}^1/_2\rangle$ resonances near the perpendicular turning point (i.e., around $g \approx 4$). The apparent *g* value of this point, $g_{\perp app}$, is given by the expansion,

$$g_{\perp app} = 2g_\perp[1 - {}^3/_{16}G'^2...], \quad G' = g_\perp\beta H_o/D \qquad (7)$$

where $g_\perp$ is the true perpendicular *g* value and $G' \leq 0.5$.

In the present circumstance, $g_{\perp app}$ is also influenced by mixing of $S \neq {}^3/_2$ states into the $M = \pm {}^1/_2$ states of the $S = {}^3/_2$ manifold. Then (Appendix 1),

$$g_{\perp app} = 2g_\perp((1 - {}^3/_{16}G'^2...) + Z/D_{eff}\, g_\perp({}^3/_{16} + 0.2044G'^2...) \qquad (8)$$

where

$$D_{eff} = d_1D_1 + d_2D_2 \qquad (9)$$

is the strong exchange limit effective *D* value for the ${}^3/_2$ state in the manifold generated from the coupled spin 2, spin ${}^3/_2$ system. In this case, the projection coefficients are $d_1 = 0$, $d_2 = -{}^3/_5$.[20] Interestingly, and somewhat surprisingly then, the *D* value of the Mn^{III} does not contribute to D_{eff} for the $S = {}^3/_2$ state. Z depends on D_1, D_2, and *J* and is given by (Appendix 1)

$$Z = \frac{8}{75|J|}[-({}^7/_2D_1 + D_2)^2 - {}^1/_7({}^{15}/_2\,D_1 - 3D_2)^2 + {}^4/_7(D_1 + D_2)^2] \qquad (10)$$

The three terms in eq 10 arise from the second-order admixtures of the $S = {}^1/_2$, ${}^5/_2$, and ${}^7/_2$ states, respectively.

In the powder pattern simulations of the excited-state 4.1 signal using an effective spin ${}^3/_2$ Hamiltonian eq 1, *D* was taken to be D_{eff}, and an effective $g_\perp$ value was used to match the central pattern edge in the perpendicular orientation to that given by eq 8. A $g_\parallel$ value of 2.0 was used in all cases, as the spectrum in the $g \approx 4$ region is insensitive to this value and the $g \approx 2$ region in PSII is always obscured by the presence of other signals.

Results

(a) Signals of the Multiline Dimer, Ground, and Excited States. In the model developed in this laboratory, three signals from the S_2 state of the OEC are assigned to the multiline Mn dimer (see Figure 9 and Discussion). These correspond to the $S = {}^1/_2$, ${}^3/_2$, and ${}^5/_2$ states of the total spin ${}^7/_2$ manifold of this center. Any parameter values inferred from modeling the spin ${}^3/_2$, 4.1 state must, of course, be consistent with the properties so far observed for the other states. The parameter most constrained is the magnitude of *J*, which must be consistent with the temperature dependences of all three states. As noted earlier, this requires $J \approx -2$ cm^{-1}.[10-12]

Figure 1a,b shows our experimental 4.1 spectra for unoriented samples at X- and Q-band, together with the simulated fits using the parameter values listed in Table 1. The main spin Hamil-

(21) Zheng, M.; Khangulov, S. V.; Dismukes, G. C.; Barynin, V. V. *Inorg. Chem.* **1994**, *33*, 382−387.

(22) Pace, R. J.; Smith, P.; Bramley, R.; Stehlik, D. *Biochim. Biophys. Acta* **1991**, *1058*, 161−170.

Table 1. Parameters of the Multiline Dimer

J (cm^{-1})[a]	D (cm^{-1})	$(E/D)_{eff}$	$\boldsymbol{g}$-tensor[d]	hyperfine projection	single-ion hyperfine parameters
2.3 (−alc)	$Mn^{III;}$ −0.9	0.02[e]	$g_\perp = 2.00$	$^2/_3$ (Mn^{III})	ref 18
>10 (+alc)	$Mn^{'IV'}$;[b] +4.0	0.066[f]	$g_\parallel = 2.0$[g]	$^1/_3$ ($Mn^{'IV'}$)	
	D_{eff}; −2.4				
	$Mn^{III} - L^+$;[c] +2.8				

[a] ±alc refers to coupling in the presence or absence of MeOH (∼2%) in buffer medium. [b] Value of D_2 assuming spin $^3/_2$ center is a Mn^{IV} ion. [c] Value for Mn^{III} ion if the $^3/_2$ center is $Mn^{III} - L^+$ system, see text. [d] Both Mn ions assumed to have same $\boldsymbol{g}$-tensor. [e] Effective value to fit present data. [f] To fit data of Haddy et al.[13] [g] Fit insensitive to minor variations.

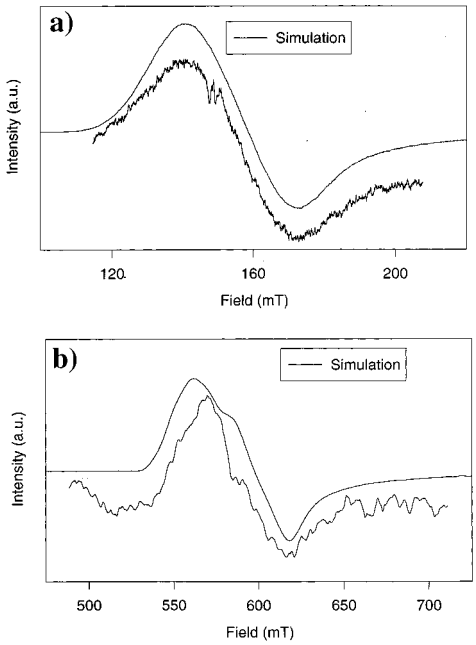

Figure 1. Experimental X-band (a) and Q-band (b) spectra of the excited-state form of the $g = 4.1$ signal, together with simulations using parameter values from Table 1 for the multiline dimer center. Spectrometer conditions: (a) frequency, 8.97 GHz; power, 11 mW; modulation frequency, 100 kHz; modulation amplitude, 1.7 mT; temperature, 9 K; simulation line width, 5 mT; (b) frequency, 34.7 GHz; power, 30 mW; modulation frequency, 100 kHz; modulation amplitude, 0.5 mT; temperature, 9 K; simulation line width, 8 mT.

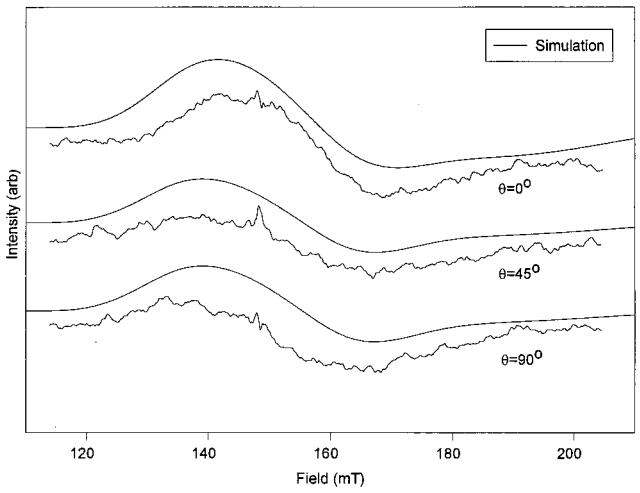

Figure 2. X-Band experimental and simulated spectra of the excited-state $g = 4.1$ signal in one-dimensionally ordered samples. Spectrometer conditions: frequency, 8.975 GHz; microwave power, 30 mW; modulation amplitude, 2 mT; temperature, 8 K; total of five scans; simulation parameters as for the powder pattern spectrum, Table 1; Line width, 5 mT. The angle indicated (θ) is the angle between the membrane plane normal and the applied field. The simulation corresponds to an orientation of the molecular axis in the membrane plane as given in Figure 10.

tonian parameters are uniquely (within a correlated uncertainty of ∼15%) established by the following requirements:

(i) The limiting low-field value of $g_{\perp app}$ is 4.30, while the value at Q-band (35 GHz) is 4.20.

(ii) The dominant term in eq 10 for Z is negative, which then requires D_{eff} to be negative, so D_2 is large positive.

(iii) The value of J, which influences $g_{\perp app}$ through eqs 8 and 10, must also be consistent with the temperature dependences of the multiline, $g \approx 4.1$ and 6 states (see below).

The X-band 4.1 spectrum appears somewhat broader in the region below $g = 2$ than does the simulation at a typical observation temperature of ∼10 K. This broadening has been shown to be due to the appearance of the next excited state,[11] near $g = 6$, and may be apparent as a separate peak in the corresponding Q-band spectrum. The fit at Q-band is not exact; however, the parameter set used to fit the spectrum is the only one, using this Hamiltonian, that will fit the spectrum at both frequencies. The discrepancies may, in part, be due to an orientation-dependent line width, which has not been included in the simulation (e.g., as in ref 13) in order to reduce the number of parameters used.

The X-band spectra of the one-dimensionally ordered samples obtained by us[10] together with their simulated best fits are shown in Figure 2. The membrane fragments were well aligned, as evidenced by the g_y, g_z components of cytochrome b-559 in the spectrum as previously observed.[19] The simulation parameters are the same as those for the powder pattern spectra (Table 1). A Gaussian distribution with a variance of 15° has been assumed for the mosaic spread of the membrane particle alignment with the plastic sheet. The simulations indicate that the molecular z-axis is close to the membrane plane ($\beta = 60°$) and that one of the perpendicular axes is nearly in the membrane plane ($\alpha = 80°$) (see Figure 10 and Discussion).

Haddy et al.[13] have also made an extensive study of the 4.1 signal from intact and inhibited systems at several frequencies, including a valuable orientation study at P-band. From the sample preparation protocols described by Haddy et al., we would expect that the 4.1 signal type generated by them in the uninhibited samples should correspond to our excited-state form. Initial fitting trials showed, however, that their spectra exhibited a somewhat greater deviation from axial symmetry than those seen here. Figure 3 shows our fit to their (reproduced) data for unoriented samples at S-, X-, and P-band. The fitting parameters are listed in Table 2. We have assumed the same Mn hyperfine values as those used in simulating our excited-state 4.1 signal form but have found it necessary to employ a Gaussian line width essentially proportional to frequency. This suggests a significant g (or D) strain component, although the line widths we employ are still significantly smaller than those employed by Haddy et al. in their simulations. Beyond the larger E/D_{eff} value, however, the spin Hamiltonian parameters are the same as those in Table 1.

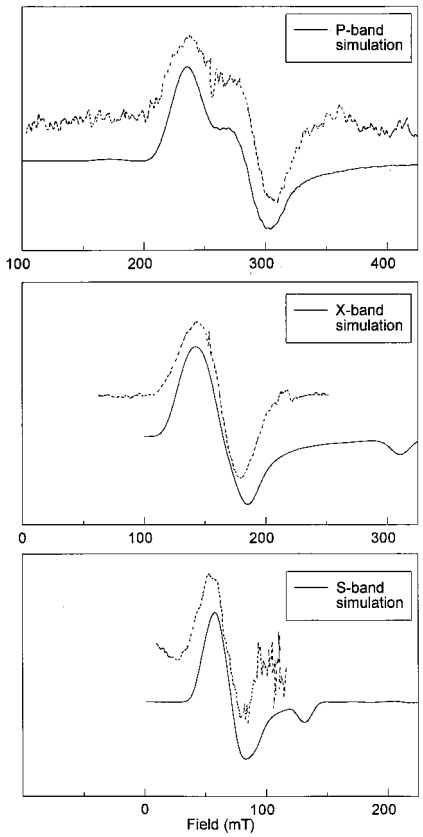

Figure 3. P-, X-, and S-band simulations of the 4.1 species signals reported by Haddy et al.[13] The dashed curves are reproductions (by kind permission of the author) of the data in ref 13, Figure 1, where the experimental conditions may be found. The simulation parameters are listed in Table 1. Line widths used in the simulations are 5 (S-band), 10 (X-band), and 15 mT (P-band).

Table 2. Parameters of the Symmetric, Radical-Bridged Mn Dimer[a]

D_{eff} (cm^{-1})	$(E/D)_{eff}$	g	hyperfine projection (Mn)	single-ion hyperfine parameters (mT)
+1.1	0.037	$g_\perp = 2.15$ $g_\parallel = 2.0$	$^1/_3$, $^1/_3$	$A_{iso} = 10$

[a] For two equal oxidation state Mn bridged by spin $^1/_2$ radical, as described in text, with net spin = $^3/_2$.

Figure 4 shows our simulation of the oriented P-band spectra. The inferred orientation of their molecular axis tensor to the membrane plane is similar to that found in our system but is distinguishable from it. The *z*-axis was found to be oriented 75° to the membrane plane normal (compared to 60° in our system) and one of the perpendicular axes 70° to the normal (compared to 80°). Generally, however, a near-axial spin $^3/_2$ state of the type invoked here appears to give a good overall fit the data of Haddy and co-workers. In particular, the slightly larger deviation from axial symmetry makes the signal orientation dependence at P-band quite marked, and this is well reproduced by our simulations. Interestingly, our simulation parameters suggest that their species should be virtually unobservable at Q-band, as the two perpendicular transitions are then separated by 150 mT and the lines very broad. This would explain a reported failure of this group to observe any Q-band signals from the 4.1 center.[13]

Figure 5 shows the fit of the existing model to the observed relative temperature dependences of the signals assigned to the three lowest net spin states of the $Mn^{III}-Mn^{IV}$ dimer. The

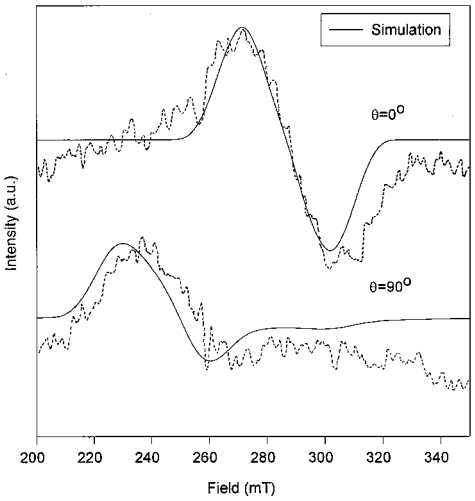

Figure 4. Simulation of P-band 4.1 signal spectra for one-dimensionally ordered samples at two orientations relative to the external field. Data from Haddy et al.[13] as in Figure 3. Simulation parameters are listed in Table 1. The simulation corresponds to an orientation of the molecular axis in which the *z*-axis is 75° to the membrane plane normal and one of the ⊥ axes 70° to the normal; compare Figure 10a.

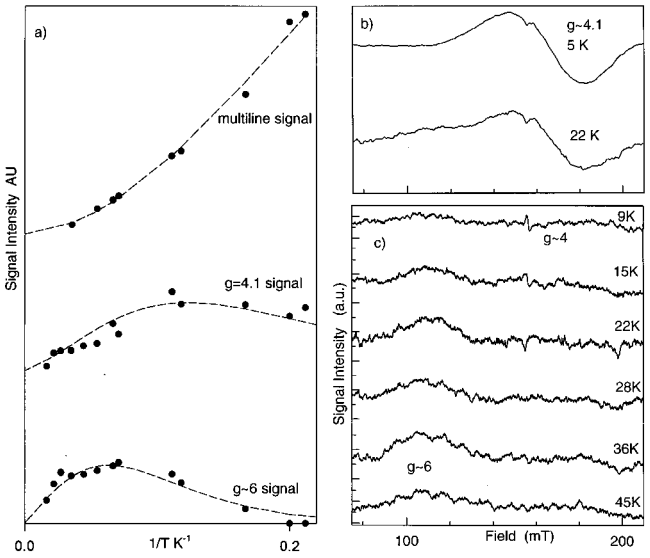

Figure 5. (a) Temperature dependences of the signal intensities of the S_2 state multiline, $g = 4.1$ and $g \approx 6$ signals. Relative signal amplitudes were determined as described earlier.[11] The broken lines are Boltzmann fits to the data using energy levels from eq 11 and Table 1. (b) The shape of the $g \approx 6$ signal which builds at high temperatures is obtained by subtracting scaled amounts of the 4.1 signal derived from the 5 K spectrum. (c) Temperature dependence of $g = 4.1$ subtracted spectra in the range 10−50 K. A discernible structure appears in the range 100−200 mT at temperatures above 30 K. This may be composed of doublets, with spacing of 4−5 mT. The structured signal appears to overlay the $g \approx 6$ resonance, rather than be part of it, based on a differential temperature development of the two species. Experimental conditions are as described in ref 11.

relative energy levels are determined mostly by the value of J (as in eq 1) but modified somewhat by the fine structure terms. These effects have been included to first order and have their largest influence on the spin $^3/_2$ (4.1 signal) state. In all cases, the signal is assumed to arise from transitions within the $M = \pm^1/_2$ levels of the relevant net spin state. The relative energy level expression is then

$$E_{s,m} = -JS(S+1) + D_S[M_S^2 - {}^1/_3 S(S+1)] \quad (11)$$

where the D_S terms are the first-order effective values for each S level, calculated in the strong exchange limit (e.g., as in eq 9, see ref 20). Parameter values are from Table 1. There are four net spin states ($^1/_2$,$^3/_2$, $^5/_2$, $^7/_2$) predicted to arise from the III−IV dimer model of the Mn pair which gives rise to the multiline. We have described previously[11] our procedure for quantitating the first three of these (multiline, $g = 4.1$ and $g \approx 6$). The multiline signal is well removed from the rest, but the $g \approx 4.1$, $g \approx 6$, and $g \approx 8$ signals anticipated from the spin $^7/_2$ state overlap at X-band. We estimate the $g \approx 6$ signal by appropriate subtraction of the $g \approx 4.1$ component, as indicated in Figure 5b. Figure 5c shows the resulting, isolated $g \approx 6$ signals as a function of temperature. It is probable that a hyperfine structured component forms over this at temperatures above 30 K. This structure appears to be composed of partially resolved doublets, of spacing ∼4 mT. This behavior is qualitatively what one would expect from the highest (spin $^7/_2$) state in the manifold, in which the hyperfine projection terms are both ∼0.5. That the pattern appears not to be centered on $g \approx 8$ is not surprising, as the effective fine structure term for the $S = {}^7/_2$ state is small (∼0.3 cm^{-1}), resulting in a system no longer in the low-field limit, even at X-band. These signals are currently under further study.

Last, there is an interesting and unexpected consequence that arises from the numerical values of D_1 and D_2. This concerns the Mn hyperfine pattern of the multiline spin $^1/_2$ state. It is well known that the multiline pattern is little influenced, in general shape, by the presence or absence of alcohol in the buffer medium. In our interpretation, small mono-alcohols (particularly MeOH), when present at the few percent level, increase the magnitude of J to the point where the 4.1 state is no longer visible at temperatures ≤30 K (refs 10, 11, and 18 and below; i.e., the strong exchange limit is approached). Normally one would expect the multiline pattern to be significantly altered by this modulation of J, as second-order interactions normally have a strong influence on the hyperfine pattern of the spin $^1/_2$ ground state of a dimer when D/J is of order unity.[21] This is normally interpreted as a J dependence of the effective hyperfine coupling constants of the two ions. In the present case, such an interpretation is inappropriate, due to the strong quadrupole effects on both ions which we have inferred from our modeling of the S_2 state.[18] However, a second-order perturbation treatment (Appendix 2) of the hyperfine energy levels in the ground (spin $^1/_2$) state under these circumstances still yields a result formally similar to that derived earlier.[21] In particular, the functional dependence of the average hyperfine line position shift (Δ_{hf}) is of the form

$$\Delta_{hf} \sim \frac{1}{3J}(7D_1 + 2D_2)A_{\perp av} \qquad (12)$$

where $A_{\perp av}$ is an average single-ion perpendicular direction hyperfine coupling constant (∼−11 mT from our previous modeling[18]). Normally, for a conventional set of D_1 and D_2 parameter values ($|D_1|$ (Mn^{III}) ≈ 2−3 cm^{-1}, $|D_2| \leq 0.5$ cm^{-1}), the bracketed term in eq 12 is ∼15−20 cm^{-1} in magnitude, leading to a large effect on the hyperfine coupling constant whenever $|J|$ is ≤10 cm^{-1}. In the present case, however, the bracketed term in eq 12 is only ∼1.5 cm^{-1}, or even less. Since the sign of this term is positive, Δ_{hf} is a shift away from the pattern center ($g = 2$) of ∼0.2 mT on average. Comparison of the upfield and downfield multiline hyperfine patterns for PSII material in the presence (high J, strong coupling) and absence (low J, weak coupling) of MeOH[22] shows that the spectra are quite similar but exhibit numerous subtle differences. In the downfield region, which displays the simpler, more regular structure, an average shift of the magnitude suggested by eq 12 appears to be evident. As noted above, to the extent that eq 6 is valid, there is no second-order perturbation of the apparent g value of the multiline. We have already shown from X- and Q-band comparisons that the $\boldsymbol{g}$ tensors of the plus and minus alcohol forms of the multiline signal are very similar.[10]

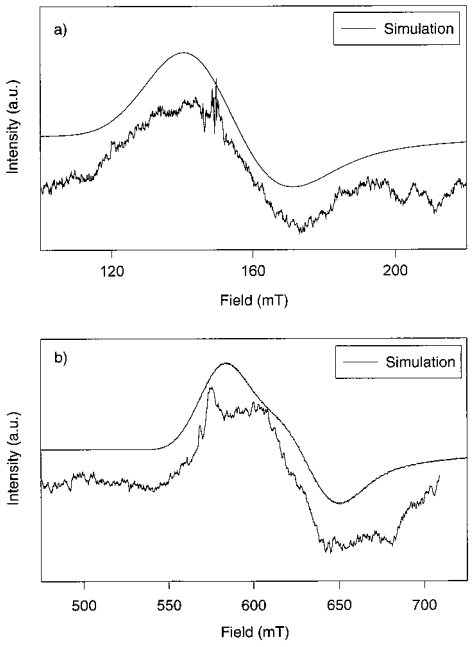

Figure 6. Experimental X-band (a) and Q-band (b) spectra of the ground-state form of the $g = 4.1$ signal, together with simulations using parameter values from Table 2 for the inner, radical-bridged dimer center. Experimental conditions are as in Figure 1. Simulation line widths: (a) 13 (b) 18 mT.

(b) 4.1 Ground-State Signal of the Second Dimer. Smith and Pace have proposed a symmetric trinuclear cluster,[11] containing a radical-bridged Mn homodimer as the center, giving rise to the ground 4.1 signal. This was inspired by the analysis of Brudvig and co-workers.[23,24] Other spin states (beyond the ground $S = {}^3/_2$ states) have now been detected from this center,[12] indicating that both the J_{12} and $J_{1,23}$ (=J') couplings are at least 50 cm^{-1} in magnitude. These estimates place the interaction between the manganese in the strong coupling regime ($|D/J| \ll 1$). For such a system, an expression for the contributions of the individual zero field splitting parameters together with dipolar contributions can be derived (see below).

Figure 6a and b shows the experimental, unoriented g ≈ 4.1 spectra at X- and Q-band, together with the simulation fits assuming the parameter values listed in Table 2, for an effectively isolated spin $^3/_2$ center.

The ground-state form of the spectrum at X-band is remarkably similar to the excited-state form at this frequency. At Q-band, on the other hand, it exhibits a different g-value and line shape (compare Figures 6 and 1). It was not possible to simulate this signal using the large D_{eff} value of the excited-state form. There are some subtraction artifacts in the Q-band spectrum that make determination of the line shape difficult; for instance, some rhombic iron signal remains at $g = 4.3$. Again, no orientation-dependent line width has been included. Because we have no independent information on the hyperfine parameters of the two Mn in the homodimer proposed to

(23) de Paula, J. C.; Brudvig, G. W. *J. Am. Chem. Soc.* **1985**, *107*, 2643−2648.
(24) de Paula, J. C.; Beck, W. F.; Brudvig, G. W. *J. Am. Chem. Soc.* **1986**, *18*, 4002−4009.

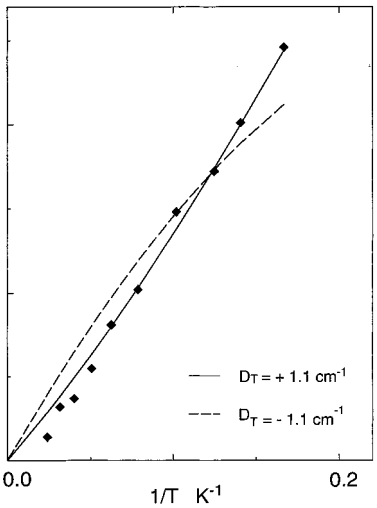

Figure 7. Temperature dependence of the ground-state 4.1 signal amplitude, determined as the low power limiting nonsaturation value, as described previously.[11] The two curves are Boltzmann fits to the data assuming D positive (solid line) and negative (dashed line). Only the two Kramer's doublet substates of the spin $^3/_2$ model for the signal are considered; possible higher states are ignored.

contribute to the ground 4.1 signal, we have arbitrarily assumed two equal isotropic couplings of 10 mT. This is the minimum value which gives a reasonable fit to the data, assuming the strong coupling limit for the projection operators. A value of ~10 mT would be more consistent with the expected range for $A_\perp$ in Mn^{III}, rather than a Mn^{IV} coupling in a conventional environment.

Both forms of the 4.1 signal exhibit near-axial fine structure with $E/D < 0.05$. It was not possible to account for the spectra at both X- and Q-band for the ground-state 4.1 signal without allowing $g_\perp$ to increase above 2.0. It is much more difficult to ascertain the value of $g_\parallel$, as the small resonance due to it appears under the tyrosine radical centered at $g = 2$. If $2D$ is smaller than $h\nu$ ($h\nu \sim 0.3$ cm^{-1}), then the feature at $g = 2$ is strong. This is clearly not the case here.

The simulations are insensitive to the sign of the effective D value (D_T) for the ground spin $^3/_2$ state. However, if D_T is positive, then the $M = \pm^1/_2$ states which give rise to the $g \approx 4$ resonance lie $2D_T$ below the $M = \pm^3/_2$ states, which are generally EPR silent at X-band. If D_T is negative, this situation is reversed. Figure 7 shows the temperature dependence of the ground 4.1 signal, as determined by us.[10,11] It is clearly more consistent with a Boltzmann model assuming a positive sign for D_T.

In the case of a symmetric trinuclear cluster such as assumed here, the fine structure spin Hamiltonian parameters are related by[20]

$$\boldsymbol{D}_T = d_1\boldsymbol{D}_1 + d_2\boldsymbol{D}_2 + d_3\boldsymbol{D}_3 + d_{12}\boldsymbol{D}_{12} + d_{13}\boldsymbol{D}_{13} + d_{23}\boldsymbol{D}_{23}$$

where $\boldsymbol{D}_{12}$ etc. are cross-term (dipolar) contributions between centers.

The contribution from the radical (d_3) can be neglected, as the intrinsic D vanishes for a spin $^1/_2$ system.

The coupling coefficients can be calculated by using expressions given by Bencini and Gatteschi[20] and are $d_1 = d_2 = -^7/_{10}$ and $d_{12} = ^{13}/_{15}$, assuming $S_1 = 2$, $S_2 = 2$, $S_3 = ^1/_2$, and $S_T = ^3/_2$. The magnitude of the dipolar coupling, D_{12}, in the Mn^{III}–Mn^{III} dimer can be estimated using a simple dipole–dipole approximation to be ~0.3 cm^{-1}. The D_{13} and D_{23} terms, involving the $S = ^1/_2$ center, are expected to be smaller still.

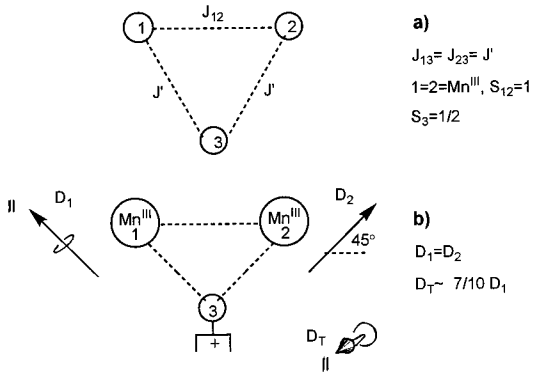

Figure 8. (a) Coupling scheme for the Mn homodimer bridged by a radical ligand proposed in ref 11 as the spin center responsible for the ground-state 4.1 species. Coupling J_{12} is antiferromagnetic, and $J_{13} = J_{23} = J'$ is ferromagnetic. When $2|J_{12}| < J' < 4|J_{12}|$, the ground state has spin $^3/_2$. (b) Possible orientation of the individual Mn ion fine structure tensors (D_1,D_2) within the three-spin system, which would lead to substantial cancellation in the resulting total fine structure tensor D_T. Both single-ion tensors are assumed to be axial and equal. D_T is then also axial and oriented as shown (parallel orientation normal to page).

Thus, the largest contribution to D_T will come from the intrinsic zero field parameters of the two Mn, as the Mn–radical dipolar contributions will be <0.1 cm^{-1}.

The relatively small value inferred for D_T, ~1.1 cm^{-1}, would imply a rather small zero field parameter for each Mn^{III}, ~0.6 cm^{-1}, if all the fine structure tensors were favorably aligned. While $|D|$ values <1 cm^{-1} have been reported for Mn^{III} in low-symmetry environments,[25] the more likely explanation for the D_T value, especially if the Mn oxidation state is +3, is that the tensors are misaligned and substantially cancel. For instance, if each Mn single-ion $\boldsymbol{D}$ tensor were aligned as in Figure 8 (with $D_\parallel$ positive and directed along the Mn–radical bond direction), the resultant system would still be quasi-axial (but with the parallel direction now out of the figure plane and of positive sign). $D_T \approx 1.1$ cm^{-1} would then require individual ion D values of ~2 cm^{-1}. This is well within the reported range for Mn^{III}, while being somewhat large for Mn^{IV}.[25]

Discussion

The strong conclusion from this study is that both forms of 4.1 signals that we have previously identified may be modeled as near axial spin $^3/_2$ systems. This supports our earlier assignment[10–12] of these spin states and the "separate dimers" model given in refs 11, 12, and 18. Here we discuss briefly the implications for that model of the various site parameters obtained here, as well as addressing recent work of others, some of which appears to support and some to challenge our picture. We consider first the Mn site parameters, particularly for the dimer giving rise to the multiline and excited-state $g = 4.1$ signals, as these parameters have a direct bearing on subsequent discussion.

Mn Site Parameters. Within the limits of the model we have imposed (i.e.,eq 5), the D_1 and D_2 parameter values for the multiline dimer are overdetermined by the data examined here. The sign and value of D_1 are consistent with a Mn^{III} ion in a quasi-axial environment and $^5B_1$ ground electronic state (i.e., electron in the d_{z^2} orbital). The relatively small magnitude (~1 cm^{-1}) of the term, which is little more than the spin–spin

(25) Al'tshuler, S. A.; Kozyrev, B. M. *Electron paramagnetic resonance in compounds of transition elements*, 2nd rev. ed.; John Wiley & Sons: New York, 1974.

interaction alone for Mn^{III} ($\sim$0.6 cm^{-1}),[26] suggests that the intermediate spin-excited t_2^4 configuration is well removed from the ground state.[27] This then is totally consistent with only a modest ligand field directed along the *z* (i.e., parallel) axis for this ion, i.e., it is ligand deficient in this direction. Such is precisely the conclusion we reached earlier from modeling the hyperfine interactions within the multiline state.[18]

The large value of D_2, $\sim$4 cm^{-1}, presents a puzzle if it is interpreted to apply to a Mn^{IV} (d^3) ion. The single-ion hyperfine tensor for this species inferred from the multiline simulations was also most unusual for Mn^{IV}, being large and anisotropic. Both are plausible, however, for d^4 Mn^{III}! This raises the interesting possibility that the net spin $^3/_2$ center which the EPR modeling requires for this species is, in fact, a Mn^{III}−radical pair, strongly antiferromagnetically coupled. The radical would presumably be an oxidized ligand. This would be the species which actually undergoes oxidation on the S_1-to-S_2 transition. We would then interpret the XANES Mn edge shift seen on this transition[28] as arising from an altered ligand environment of a Mn^{III}. It has been noted[29] that only Mn^{II} appears to possess a XANES shape uniquely characteristic of its oxidation state. Further, a Mn^{III}−Mn^{III} combination in S_2 would then explain the relatively weak ($|J| \leq 10$ cm^{-1}) antiferromagnetic coupling inferred for the multiline signal species, which would be, to our knowledge, unprecedented for a true Mn^{III}−Mn^{IV} dimer with an internuclear separation of less than 3 Å.

Examples of antiferromagnetically coupled high-valent Mn−radical ligand systems with unusual, anisotropic Mn hyperfine couplings have recently been described.[30] These involve complexes of a metal (Mn, Fe, Co) in the III or IV oxidation state with semiquinone ligands, in particular Schiff base biquinone radical ligands[30−34] Modeling of the EPR spectrum of the Mn^{IV} diradical species[30] shows that the radical ligand couples antiferromagnetically and induces a large, axially anisotropic hyperfine effect at the Mn nucleus. This must be negative in sign, with the parallel axis directed along the Mn−N bond in the case of the Schiff base species. In addition, the isotropic Mn nuclear coupling is increased in magnitude ($\geq$10 mT), well above that seen for Mn^{IV} in conventional ligand environments ($A_{iso} \approx 7$ mT). All of these factors are consistent with the assignment of the "Mn^{IV}" species in the multiline dimer as being actually a Mn^{III}−radical pair, with the hyperfine *y*-axis (Figure 10 and ref 18) pointing essentially along the Mn−radical bond direction. The nature of the radical is as yet uncertain, histidine or tyrosine side chains being obvious possibilities. The true single-ion *D* value for the Mn^{III} center in the coupled system would be $\sim$+ 2.7 cm^{-1}.[20] The positive sign suggests a ground state of mostly $^5A_1$ character, but the hyperfine symmetry[18] is more indicative of $^5B_1$, with an axial ligand radical contribution superimposed along one perpendicular direction. Jiang et al.[35] have shown that d^4 systems in the same ground state may exhibit either sign of *D* as a consequence of unusual combinations of tetragonal distortion parameters mixing different combinations of excited-state components. Some such effect may be occurring here.

For the two Mn (probably oxidation state III) associated with the electron-transfer radical, little further can be presently said. Only the sign and magnitude of D_T is known. It is expected that a detailed study of the excited states predicted for this system will be more revealing (Smith and Pace, manuscript in preparation).

Mn Organizational Model. Figure 9 summarizes the model of the Mn organization in the OEC which has emerged in our work. In particular, we indicate our assignment of the states responsible for all the Mn derived or related EPR signals known from the OEC in its functional, uninhibited form. This is a total of at least seven signals. We have discussed above in detail our interpretation of four of these signals. Data on the remaining three have, for the most part, emerged only very recently. However, all appear to us to have an interpretation within the scheme illustrated in Figure 9, at least qualitatively. We consider them in turn.

(i) S_0-State Signals. Åhrling et al.[36] and Messinger et al.[37] have shown that a multiline-like Mn hyperfine structured EPR signal is visible in the S_0 state of the OEC, in the presence of small (a few percent) concentrations of MeOH. The latter is necessary for observation of the structured signal. The data of Åhrling et al., which were obtained from totally physiological, multiple flash turnover to the S_0 state, reveal a signal which is at least 40 mT wider than the conventional S_2-state multiline. As pointed out by those authors, this is essentially the magnitude of pattern width increase to be expected in a Mn^{II}−Mn^{III} dimer, assuming single-ion hyperfine parameters inferable from those employed in the simulations of the S_2 state,[18] although detailed simulations of the S_0-state signal are yet to be performed. The crucial role of MeOH in stabilizing what must be an antiferromagnetically coupled net spin $^1/_2$ state in S_0 is interesting. We have long maintained[10−12,18,22] that small mono-alcohols, MeOH in particular, modulate the exchange coupling in the multiline dimer, possibly by influencing the state of protonation of bridging oxo groups. In the presence of alcohols, the coupling is shifted in the antiferromagnetic direction, which is known from model compounds to occur with oxo-bridge deprotonation.[38] In the absence of MeOH, the very weak antiferromagnetic coupling of the S_1 state (III−III) probably becomes net ferromagnetic in S_0 (II−III). The resulting spin $^9/_2$ ground state would be difficult to observe with EPR and might be invisible at X-band.

(ii) S_1-State Signals. Kawamori et al.[17] have recently confirmed the existence of a $g \approx 5$ signal in the S_1 state, observable with parallel polarization ($\Delta m_S = 0$ transition). This was first seen by Dexheimer and Klein[16,39] but subsequently not found by others. Kawamori et al. have confirmed the

(26) Abragam, A.; Bleaney, B. *Electron paramagnetic resonance of transition ions*; Dover Publications Inc.: Mineola, NY, 1986.
(27) Gerritsen, H. J.; Sabisky, E. S. *Phys. Rev.* **1963**, *132*, 1507−1512.
(28) Roelofs, T. A.; Lian, W.; Latimer, M. J.; Cinco, R. M.; Rompel, A.; Andrews, J. C.; Sauer, K.; Yachandra, V. K.; Klein, M. P. *Proc. Natl. Acad. Sci. U.S.A.* **1996**, *93*, 3335−3340.
(29) Riggs-Gelasco, P. J.; Mei, R.; Penner-Hahn, J. E. In *Mechanistic Inorganic Chemistry*; Thorp, H. H., Pecoraro, V. L., Eds.; Advances in Chemistry Series 246; American Chemical Society: Washington, DC, 1995; pp 219−248.
(30) Swarnabala, G.; Rajasekharan, M. V.; Padhye, S. *Chem. Phys. Lett.* **1997**, *267*, 539−544.
(31) Kessel, S. L.; Emberson, R. M.; Debrunner, P. G.; Hendrickson, D. N. *Inorg. Chem.* **1980**, *19*, 11770-1178.
(32) Larsen, S. K.; Pierpont, C. G. *J. Am. Chem. Soc.* **1988**, *110*, 1827−1832.
(33) Ahia, A. S.; Pierpont, C. G. *Inorg. Chem.* **1995**, *34*, 1172−1179.
(34) Ahia, A. S.; Jung, O.-S.; Pierpont, C. G. *Inorg. Chim. Acta* **1994**, *226*, 91−98.
(35) Jiang, C.-Y.; Du, M.-L.; Zhou, Y.-Y. *Phys. Rev. B* **1994**, *50*, 949−954.
(36) Åhrling, K. A.; Peterson, S.; Styring, S. *Biochemistry* **1997**, *36*, 13148−13152.
(37) Messinger, J.; Nugent, J. H. A.; Evans, M. C. W. *Biochemistry* **1997**, *36*, 11055−11060.
(38) Baldwin, M. J.; Stemmler, T. L.; Riggs-Gelasco, P. J.; Kirk, M. L.; Penner-Hahn, J. E.; Pecoraro, V. L. *J. Am. Chem. Soc.* **1994**, *116*, 11349−11356.
(39) Dexheimer, S. L.; Sauer, K.; Klein, M. P. In *Current Research in Photosynthesis*, Vol. 1; Baltscheffsky, M., Ed.; Kluwer Academic Publishers: Dordrecht, 1990; pp 761−764.

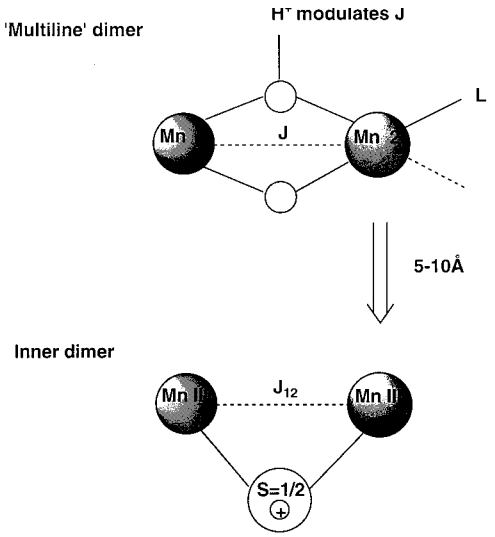

	Signal Type (Spin state)	Oxidation States Mn1	Mn2	L	Buffer MeOH
S_0	Multiline (1/2)	+2	+3	0	+
S_1	Parallel polarisation (1)	+3	+3	0	-
S_2	Multiline (1/2)	+3	+3	+1	+, -
	Excited g=4.1 (3/2)	"	"	"	-
	g~6 (5/2)	"	"	"	-
	(g~8) (7/2)	"	"	"	-

Oxidation Gives:

Ground 4.1,
Excited State 'Radical' (Y_Z?)

Figure 9. Model for the two Mn dimer structures within the OEC, summarizing the magnetic interactions and individual center oxidation states assigned to each of the eight OEC related paramagnetic signals discussed here. For the behaviors described in the text, the dimers must be magnetically isolated from each other, but within rapid electron-transfer range (5−10 Å). The bridging $S = {}^1/_2$ radical ligand species in the "inner" dimer is tentatively assigned to $Y_Z^{\bullet}$. The table gives the proposed oxidation states of the three redox centers associated with the "outer" (S-state cycling) dimer, for the signals assigned to that system. L is the putative terminal ligand which, when oxidized, is strongly antiferromagnetically coupled to Mn2 (see text), producing a net spin $^3/_2$ center. The behavior of this dimer in the S_o, S_1, S_2 states is modulated by the strength of the antiferromagnetic coupling *J*, which is influenced by MeOH (+, present (few %); −, absent; see text). It is always more strongly antiferromagnetic in the presence of MeOH, possibly reflecting deprotonation of oxo bridge(s).

Dexheimer−Klein result that the S_1 signal coexists with the 4.1 signal, but not the multiline signal, and have shown importantly that the S_1-state signal is visible as a weakly excited state in the absence of MeOH but invisible in the presence of MeOH. These observations are consistent with the model in Figure 9, assuming the parallel polarization signal arises from the first excited (spin 1) state of the multiline dimer (III−III). That both the Mn in this pair are Mn^{III}, in the S_1 *as well as* the S_2 state (see above), would explain the fact that virtually the same (a few cm^{-1}) weak antiferromagnetic coupling between them is seen in the S_1 and S_2 (multiline) states in the absence of MeOH. In the presence of MeOH, the spin 1 state is thermally inaccessible. Both sets of workers successfully modeled the parallel polarization signal as the normally forbidden half-field transition of a rhombic ($E/D \approx 0.3$) spin 1 state with small *D* (<0.2 cm^{-1}). Although the system is clearly not in the strong exchange limit, the small net magnitude of *D* (necessary for the signal to be visible at X-band) suggests near complete cancellation of the individual Mn^{III} center *D* values in the S_1 state of the OEC. As shown above, these are about −0.9 and +2.7 cm^{-1} from our S_2-state modeling, but the latter value would need to be $\sim$+1.3 cm^{-1} in S_1 following reduction of the ligand. In this regard, the very recent observation of a parallel polarization "multiline" signal in PSII from *Synechosystis* is interesting.[40] This signal, consisting of 16−18 lines of $\sim$3-mT spacing, almost certainly arises from a center similar (but with a slightly different fine structure tensor) to that giving rise to the S_1 signal in plant PSII. The simple interpretation of two Mn^{III} ions with *D* values of similar magnitude but of opposite sign is that they are subject to opposite Jahn−Teller axial distortions, and so are of equivalent but opposite hyperfine asymmetries. If $A_\perp \approx -12$ mT and $A_\parallel \approx -3$ mT for one Mn^{III} (as in ref 18, negative *D*), then $A_\perp \approx -6$ mT and $A_\parallel \approx -14$ mT for the other Mn (positive *D*). Along the perpendicular direction, which will dominate the powder pattern resonance, such a coupled system should give a 16-line hyperfine pattern with 3-mT spacing.

The quantitative inter-relation of the S_1, multiline, and 4.1 signals is one of the strongest single pieces of evidence in favor of a "separate centers" interpretation of the Mn organization within the OEC. This was recognized by Dexheimer and Klein.[16,39] Moreover, the well-established observation (refs 5, 23, 24, and 41 that interconversion between the (ground-state) 4.1 signal and the multiline signal can occur within seconds at 200 K means that electron transfer, rather than ligand/structural rearrangements, is the only plausible mechanism for this process (see below).

(iii) Tyrosine Z. Conventionally, Y_z is regarded as an isolated oxidizable intermediate electron-transfer species between the Mn cluster and the P680 reaction center.[1] Recently, Razeghifard et al.[42,43] have shown that the apparent intensity of the radical-like Y_z species during the physiological turnover of the OEC is only about 50% of that expected from the centers turning over. This intensity deficit has long been known from the work of several groups[44−46] on both functional and inhibited systems containing an intact Mn cluster but has been generally regarded as an underestimate arising from measurement limitations in the functional systems.[44,45] These limitations did not apply in the inhibited case[46] and were essentially absent in the studies of Razeghifard et al. We have recently reported[12] a radical signal in PSII that exhibits non-Curie temperature dependence below $\sim$30 K and an apparent intensity of $\sim$40% of that of the dark stable Y_D^{ox} signal and exists only in the presence of the ground-

(40) Campbell, K. A.; Peloquin, J. M.; Pham, D. P.; Debus, R. J.; Britt, R. D. *J. Am. Chem. Soc.* **1998**, *120*, 447−448.

(41) Boussac, A.; Girerd, J.-J.; Rutherford, A. W. *Biochemistry* **1996**, *35*, 6984−6989.

(42) Razeghifard, M. R.; Pace, R. J. *Biochim. Biophys. Acta* **1997**, *1322*, 141−150.

(43) Razeghifard, M. R.; Klughammer, C.; Pace, R. J. *Biochemistry* **1996**, *36*, 86−92.

(44) Cole, J.; Sauer, K. *Biochim. Biophys. Acta* **1987**, *891*, 40−48.

(45) Hoganson, C. W.; Babcock, G. T. *Biochemistry* **1988**, *27*, 5848−5855.

(46) Andreasson, L.-E.; Vass, I.; Styring, S. *Biochim. Biophys. Acta* **1995**, *1230*, 155−164.

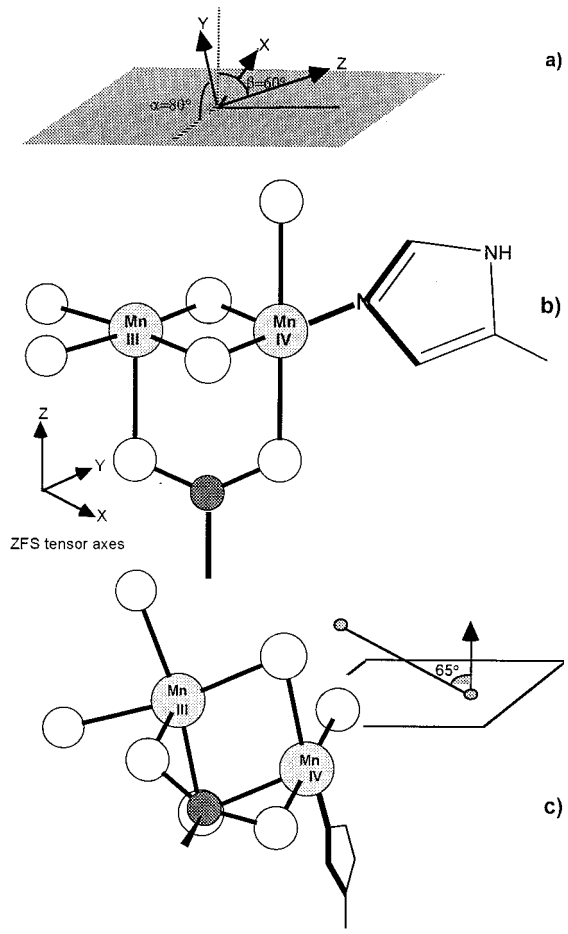

Figure 10. (a) Orientation in the membrane plane of the molecular fine structure tensor for the excited state form of the $g = 4.1$ signal, inferred from fitting the ordered spectra in Figure 2. Assuming (b) that the dimer molecular geometry and axis system are the same as those proposed earlier from modeling the multiline hyperfine pattern, the resulting configuration of the "multiline" dimer in the membrane plane is shown in (c). This gives an orientation of the Mn−Mn vector relative to the membrane normal as shown (65° angle). We have assumed, for illustrative purposes, that the oxidizable side chain, L, is a histidine (as earlier[18]). The neighboring vacant ligand position is possibly the site of (weak) Cl^- binding.

state 4.1 signal. Such behavior is consistent with this radical being the putative bridging species of the Mn pair, giving rise to the ground-state $g = 4.1$ signal (Figure 9). The radical CW spectrum at X-band resembles that reported for $Y_z^\bullet$ in Mn-intact PSII.[45] This matter is currently under further study in our laboratory (Smith et al., manuscript in preparation).

Multiline Dimer Orientation. Assuming that D_{eff} here is dominated by the Mn^{III}−radical single-ion tensor, one would expect the molecular axis parallel direction to be along the quasi-axial *z*-axis in the dimer model of the multiline center which we have previously proposed. This is reproduced in Figure 10b. Together with the tensor orientation deduced from the aligned spectra (Figure 10a), our proposal for the multiline dimer geometry, relative to the membrane plane, is shown in Figure 10c. This gives an orientation of the Mn−Mn vector to the membrane plane normal of ∼65 ± 3°, which is close to the 67° orientation found by Dau et al. from EXAFS[47] of that Mn−Mn vector influenced by ammonia binding.

As discussed above, we have interpreted the apparently variable antiferromagnetic coupling in the multiline dimer in terms of buffer-modulated protonation effects, possibly affecting the oxo bridges. When $|D/J|$ is of order unity, the magnitudes of all the effective parameters (fine structure, hyperfine coupling, etc.) in the spin Hamiltonian become sensitive to *J*. Thus, the modest differences, essentially a slightly greater deviation from axial symmetry for D_{eff} we infer between the forms of the excited-state 4.1 signal observed by Haddy et al. and ourselves, may have their origins in nothing more than slightly different site geometry/coupling states brought on by subtle differences in local protonation environments. These would derive, presumably, from as-yet unidentified differences in our respective sample preparation protocols.

Mn Structure: Separate Dimers or Tetranuclear Complex? Although we find that a dimer pair model allows a consistent rationalization of many data on the Mn organization within the OEC, several studies appear to present results strongly challenging this view. First, Boussac and colleagues[41] have reported that near-infrared radiation may induce a transformation from the multiline form to the 4.1 signal form of a PSII sample previously trapped in the S_2 state by 200 K illumination. The resulting 4.1 signal species is almost certainly the ground-state form, as the interconversion occurs optimally at near-IR illumination temperatures of ∼130−150 K and the 4.1 signal relaxes back to the multiline on brief 200 K dark annealing. Although the authors choose to discuss their results in terms of valence reorganization within a tetranuclear cluster, their observation would be consistent with our model if one assumed simply that the near-IR radiation photoexcited an electron transfer from the Mn dimer, producing the ground 4.1 signal to the multiline dimer, with the latter initially in the S_2 oxidation state. This is not the normal thermodynamically favored electron-transfer flow, as the inner pair (functionally closer to P680) probably does form part of an electron-transfer pathway and 200 K annealing allows back-reaction to the more stable redox distribution between the two Mn dimer centers.

The EXAFS data relevant to the present discussion concern the 3.3-Å (3.6-Å by some analyses[4,48]) peak in the Mn pattern. If this represents a Mn−Mn distance, then the Mn cluster is essentially tetranuclear and the model in Figure 9 is wrong. If it is a Mn−Ca interaction, however, then separate dimer models, of which ours is but one, are admitted. There is insufficient difference in the X-ray scattering properties of Ca and Mn to decide this directly.[4,48] The approaches taken to date have involved Ca^{2+} removal and/or replacement with an appropriate chemically similar, stronger scatterer (usually Sr^{2+})[48−50]. The data are as yet contradictory. Penner-Hahn and colleagues[50] see no change in the Mn EXAFS pattern of PSII following Ca^{2+}/Sr^{2+} exchange. Evans and co-workers[48] observe a decrease in the 3.6 (3.3)-Å peak on Ca^{2+} depletion. Using a different, probably more severe, depletion/exchange protocol, Yachandra et al.[49] see both an elimination of the 3.3-Å peak on Ca^{2+} depletion and an enhanced peak amplitude (with slight distance increase) on Sr^{2+} reconstitution. Their data analysis is consistent with the 3.3-Å peak being purely a Mn−Ca interaction, or a mixture of Mn−Mn and Mn−Ca interactions. Although the Berkeley group is inclined to the latter interpretation, a conservative conclusion from these studies is that separate dimer models are not excluded by the EXAFS data at this time.

(47) Dau, H.; Andrews, J. C.; Roelofs, T. A.; Latimer, M. J.; Liang, W.; Yachandra, V. K.; Sauer, K.; Klein, M. P. *Biochemistry* **1995**, *34*, 5274−5287.

(48) MacLachlan, D. J.; Nugent, J. H. A.; Evans, M. C. W. *Biochim. Biophys. Acta* **1994**, *1185*, 103−111.

(49) Latimer, M. J.; DeRose, V. J.; Mukerji, I.; Yachandra, V. K.; Sauer, K.; Klein, M. P. *Biochemistry* **1995**, *34*, 10898−10909.

(50) Riggs-Gelasco, P. J.; Mei, R.; Ghanotakis, D. F.; Yokum, C. F.; Penner-Hahn, J. E. *J. Am. Chem. Soc.* **1996**, *118*, 2400−2410.

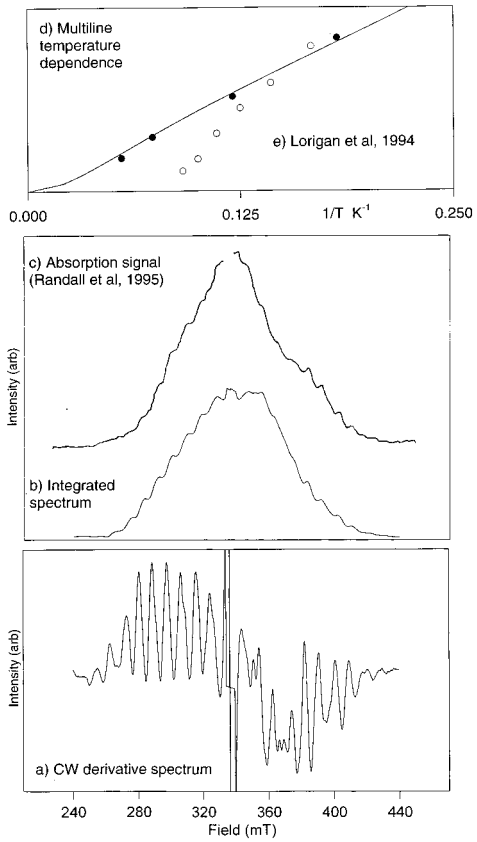

Figure 11. (a) Light-minus-dark CW spectrum of the multiline signal in PSII (5% ethanol in buffer) typically observed by us (e.g., see ref 11 for preparation details). No background signal subtraction has been applied. (b) Integrated spectrum from (a). A small, linear baseline leveling correction has been applied. The spectrum is distorted close to $g = 2.00$ due to subtraction artifacts from signal II. Spectrometer conditions: frequency, 9.42 GHz; microwave power, 6.35 mW; modulation frequency, 100 kHz; modulation amplitude, 2 mT; temperature, 8 K. (c) Trace of field-swept two-pulse echo spectrum of multiline region illuminated-minus-dark signals (5% EtOH) taken from Figure 6 from ref 51, on the same horizontal scale as (a, b) and aligned at $g = 2.00$. (d, e) Temperature dependences of "multiline" signal intensity. Data from refs 22 (CW peak height estimates, with 3% MeOH, closed symbols) and 56 (electron spin−echo, illuminated-minus-dark, 5% EtOH, open symbols). Vertical scale is arbitrary in both cases. The curve in (d) was drawn from a boltzmann model of the multiline center (as in ref 22), assuming $3|J| = 30$ cm^{-1}. Figure 6 from ref 51 reprinted with permission. Copyright 1995 American Chemical Society.

The third set of results by Britt et al.[51] concerns the observation of ^{55}Mn pulsed ENDOR from the multiline center in PSII. The ENDOR is claimed to be inconsistent with a mixed-valence Mn heterodimer, and they suggest instead a multinuclear structure involving mainly Mn^{IV}. Since the pulsed ENDOR experiment operates on the total absorption (not derivative) EPR signal, it is important to ensure that only the signal of interest (i.e., here the conventional multiline) is being detected or interpreted. Featureless background contributions, which may be irrelevant in conventional, derivative detection, here intrude. Figure 11a shows the normal CW derivative spectrum of the multiline (illuminated − dark) that we observe in the presence of 5% ethanol. The integrated, equivalent absorption spectrum is shown in Figure 11b. This displays a characteristic, near-symmetrical flat-topped trapezoidal shape we have noted earlier (ref 18, Figure 6) and is reproduced by our multiline simulation. The shape is similar to that seen by Hansson et al. (ref 7, Figure 5), also from integrated CW spectra on ethanol (4%) containing PSII, and indeed very similar to the first example of a two-pulse, field-swept, light-induced multiline spectrum from PSII (5% ethanol), reported by the Berkley group (ref 52, Figure 3). It is *not*, however, similar to subsequently reported field-swept S_2-state spectra from Britt and co-workers (refs 53, Figure 1; 54, Figure 3c; 51, Figure 6), including, in particular, that related to the pulsed ENDOR work.[51] These latter spectra (also 5% ethanol) appear to contain at least two components. This is apparent in Figure 11c, which we have traced from Figure 6[51] and aligned with Figure 11b at $g = 2.00$. One of the components in Figure 11c is unquestionably the conventional multiline signal, but the other is nonsymmetrical and may be quasi-axial with $g_\perp \approx 2.0$ and $g_{||} \approx 2.2$ (rough estimates only). This latter signal is photoinduced in the S_2 state and presumably derives from Mn. We have noted previously[22] that, in sucrose buffer without alcohol, the 200 K illumination-generated multiline signal has a broad underlying component of roughly axial shape (e.g., ref 22, Figure 10). Alcohols (2−5% in buffer) suppress this signal, but in our hands ethanol achieves this to a variable extent (only sometimes completely[18]), while methanol (2−3%) generally eliminates the signal (e.g., ref 22, Figure 1). The broad signal appears to be present in many published photogenerated, $g = 2$ region spectra of PSII and becomes prominent, even in ethanol-containing samples, with NH_3 treatment (e.g., ref 55, Figures 2 and 3). Unless such a component rigorously subtracts in the illuminated-minus-dark procedure used for isolating S_2-state signals, substantial contamination of the presumed S_2-state signal can occur when the signal is viewed in absorption mode. Likely intrusions of such effects are apparent when other pulsed EPR data are considered.

It is well established that the multiline is a spin $^1/_2$ ground state and that, in the presence of alcohols, it exhibits simple, essentially "isolated-state" Curie behavior below ~25 K.[22] Figure 11d shows a plot of the temperature dependence of the multiline signal, determined by saturation-corrected peak height measurements of CW data on MeOH containing PSII.[22] Plotted also are electron spin−echo (ESE) amplitude (illuminated-minus-dark) results for the "multiline" state taken from ref 56. The CW data exhibit the simple, near-proportional inverse temperature dependence expected for a spin $^1/_2$ ground state separated from the next highest state by ~30 cm^{-1}.[22] The behavior of the ESE data is not simple, however. Rather it implies some significant admixture (possibly negative in this instance) of a non-Curie component, whose temperature dependence is "flat" between about 5 and 15 K. This is the type of dependence we have described earlier[22] for the broad $g \sim 2$ component variably suppressed by alcohol and discussed above.

At present, we are unable to speculate further on the nature of the broad signal, beyond those thoughts we have previously offered.[18] However, since the ^{55}Mn ENDOR reported in ref 51 was all derived from the top (near $g = 2$) of the multiline (and broad) signals, it is unclear from which species it originates,

(51) Randall, D. W.; Sturgeon, B. E.; Ball, J. A.; Lorigan, G. A.; Chan, M. K.; Klein, M. P.; Armstrong, W. H.; Britt, R. D. *J. Am. Chem. Soc.* **1995**, *117*, 11780−11789.

(52) Britt, R. D.; Zimmermann, J.-L.; Sauer, K.; Klein, M. P. *J. Am. Chem. Soc.* **1989**, *111*, 3522−3532.

(53) Britt, R. D.; Lorigan, G. A.; Sauer, K.; Klein, M. P.; Zimmerman, J. *Biochim. Biophys. Acta* **1992**, *1040*, 95−101.

(54) Gilchrist, M. L.; Lorigan, G. A.; Britt, R. D. In *Research in Photosynthesis*, Vol. II; Murata, M., Ed.; Kluwer Academic Publishers: Dordrecht, 1992; pp 317−320.

(55) Andreasson, L.-E.; Hansson, Ö.; von Schenk, K. *Biochim. Biophys. Acta* **1988**, *936*, 351−360.

(56) Lorigan, G. A.; Britt, R. D. *Biochemistry* **1994**, *33*, 12072−12076.

and claims that the ENDOR proves a multinuclear Mn geometry for the OEC are premature.

Finally, we observe that Junge and co-workers have recently[57] shown that data from several groups on electrochromic band shift and EPR relaxation measurements converge on a spatial model of the redox centers in the OEC in which the "Mn cluster" and Y_z are well separated (~15 Å). This appears inescapable, as the electrochromic effects of Y_z and S_1 ($\rightarrow S_2$) oxidation on the P680 electrochromic reporter are qualitatively different, suggesting that these two redox centers subtend an angle of at least 45° with P680. The "Mn cluster" relevant here is that which stores the oxidizing equivalent on the $S_1 \rightarrow S_2$ transition in normal functional turnover (i.e., the multiline dimer in the model of Figure 9). However, Britt and co-workers have claimed from pulsed ENDOR studies[58] that Y_z is close (~4 Å) to *a* Mn center in samples inhibited by Ca^{2+} removal through low-pH citrate treatment. This procedure is functionally reversible on Ca reconstitution[59] and does not displace Mn or peripheral polypeptides. Although a dramatic conformational change on Ca^{2+} removal cannot, at this point, be excluded, the model in Figure 9 provides a natural resolution of this apparent paradox. The Mn "center" being inferred in the echo ENDOR experiments is *not* that responsible for the $S_1 \rightarrow S_2$ transition. This possibility has also been suggested by Junge et al.[60]

Acknowledgment. We thank A. Haddy for permission to reproduce experimental results on 4.1 signals. We are also grateful for useful discussions with R. Bramley. K.Å. acknowledges receipt of an Australian Postgraduate Research Award. K.Å. and P.S. acknowledge support from the Plant Science Centre. This work was supported by the Australian Research Council.

Note Added in Proof

Two very recent reports bearing on matters relevant to this study have come to our notice. These concern the dinuclear Mn center in the bacterial manganese catalase from *Thermus thermophilus*. A preliminary description of the active-site crystal structure[61] shows a ligand environment and geometry quite similar to that suggested in Figure 9 for the "multiline dimer". Further, Michaud-Soret et al.[62] report that, in the $Mn^{III}-Mn^{III}$ oxidation state of the catalase enzyme, the center can be either strongly ($J \approx -100$ cm^{-1}) or weakly ($J \approx -2$ cm^{-1}) antiferromagnetically coupled, depending probably on the degree of bridge protonation. Remarkably, when $J \approx -2$ cm^{-1}, the D parameters of the two Mn^{III} ions are comparably large and *opposite* in sign (+4.8, −4.3 cm^{-1}). When the enzyme is oxidized to the actual III−IV state, the antiferromagnetic coupling is strong ($J \approx -170$ cm^{-1}).

Appendix 1

Within the coupled spin representation basis $|S,M\rangle$ ($S = {}^1/_2, ..., {}^7/_2$), the first-order solution to eq 5 for H_o along the perpendicular direction and $S = {}^3/_2$ gives for the states $|u\rangle$, $|l\rangle$, between which the g ≈ 4 resonances occur:

$$|{}^u_l\rangle = \sum_{m=-{}^3/_2}^{{}^3/_2} A_m^{(u,l)} |{}^3/_2 \mathrm{M}\rangle \qquad \text{(A1)}$$

where

$$A^u_{3/2} = A^u_{-3/2} = -\frac{1}{2\sqrt{2}}(\sin\alpha_u - \sqrt{3}\cos\alpha_u)$$

$$A^u_{1/2} = A^u_{-1/2} = -\frac{1}{2\sqrt{2}}(\sqrt{3}\sin\alpha_u + \cos\alpha_u)$$

$$A^l_{3/2} = -A^l_{-3/2} = \frac{1}{2\sqrt{2}}(\sin\alpha_l - \sqrt{3}\cos\alpha_l)$$

$$A^l_{1/2} = -\mathrm{A}^l_{-1/2} = -\frac{1}{2\sqrt{2}}(\sqrt{3}\sin\alpha_l + \cos\alpha_l) \qquad \text{(A2)}$$

$$\tan 2\alpha_{(u,l)} = -\frac{\sqrt{3}}{(1 \mp 2G')}, \quad G' = g_\perp \beta H_o / D_{\mathrm{eff}} \qquad \text{(A3)}$$

The first-order energies are

$$E^{(1)}_{(u,l)} = D_{\mathrm{eff}}\left[\pm\frac{G'}{2} - [1 \mp G' + G'^2]^{1/2}\right] \qquad \text{(A4)}$$

The $|{}^u_l\rangle$ states will couple with $|S',M\rangle$ states ($S' \neq {}^3/_2$) in the second-order energy terms, through matrix elements of the type

$$|\langle MS'|S^2_{1z}\ (\text{or } S^2_{2z})|{}^u_l\rangle|^2; \quad S' = {}^1/_2, {}^5/_2, {}^7/_2 \qquad \text{(A5)}$$

For $S' = {}^1/_2$, only $M = \pm{}^1/_2$ states couple; for others, $M = \pm{}^1/_2$ and $\pm{}^3/_2$ couple.

So,

$$|\langle MS'|S^2_{1z}|{}^u_l\rangle|^2 = [A^{(u,l)}_m]^2 |\langle MS'|S^2_{1z}|{}^3/_2 M\rangle|^2, \text{ etc.} \qquad \text{(A6)}$$

The matrix elements on the right of eq A6 are readily evaluated using the Wigner−Eckart theorem and the reduced matrix elements for the single-center spin operators given by Scaringe et al.[63]

Then,

$$g_{\perp\mathrm{app}} = \frac{1}{\beta H_o}[(E^{(1)}_u - E^{(1)}_l) + (E^{(2)}_u - E^{(2)}_l)]$$

to second order (A7)

The first-order energy differences are obtained from eq A4, while the second-order corrections involve terms containing the differences $[A^u_m]^2 - [\mathrm{A}_m{}^l]^2$.

Expanding both as series in G' (assumed ≤0.5) gives eq 8.

The analysis neglects nonaxiality in the two centers. The simulations, assuming an effective spin ${}^3/_2$ system, require a small nonaxiality with $E/D_{\mathrm{eff}} \leq 0.05$. This will have only a very small effect on the second-order energies and means simply that the $g_{\perp\mathrm{app}}$ value given in eqs 7 and 8 is the central value about which the two slightly inequivalent $g_\perp$ values (for the *x*- and *y*-directions) are split. To second order in small quantities, this splitting is field independent.

(57) Mulkidjanian, A. Y.; Cherepanov, D. A.; Haumann, M.; Junge, W. *Biochemistry* **1996**, *35*, 3093−3107.

(58) Gilchrist, M. L.; Ball, J. A.; Randall, D. A.; Britt, R. D. In *Photosynthesis: From Light to Biosphere*, Vol. II; Mathis, P., Ed.; Kluwer Academic Publishers: Dordrecht, 1995; pp 223−228.

(59) Ono, T.-A.; Inoue, Y. *Biochim. Biophys. Acta* **1989**, *9973*, 443−449.

(60) Ahlbrink, R.; Haumann, M.; Cherepanov, D.; Bögerhausen, O.; Mulkidjanian, A.; Junge, W. *Biochemistry* **1998**, *37*, 1131−1142.

(61) Barynin, V. V.; Hemmpstead, P. D.; Vagin, A. A.; Antonyuk, S. V.; Melik-Adamyan, W. R.; Lamzin, V. S.; Harrison, P. M.; Artymiuk, P. J. *J. Inorg. Biochem.* **1997**, *67*, 196.

(62) Michaud-Soret, I.; Jacquameet, L.; Debaecker-Petit, N.; Le Pape, L.; Barynin, V. V.; Latour, J.-M. *Inorg. Chem.* **1998**, *37*, 3874−3876.

(63) Scaringe, R. P.; Hodgson, D. J.; Hatfield, W. E. *Mol. Phys.* **1978**, *35*, 701−713.

$$g_{\perp(x,y)} \approx 2g_{\perp}\left(1 - \frac{3}{16}G'^2 \mp \frac{3}{2}\left(\frac{E}{D}\right) - \frac{3}{4}\left(\frac{E}{D}\right)^2 ...\right) \quad \text{(A8)}$$

Appendix 2

Previous modeling of the multiline pattern[18] indicates that the hyperfine tensors for both Mn centers are rhombically distorted quasi-axial, with $A_{x,y} > A_z$. The pattern, over most of its width, is dominated by the $A_{x,y}$ values and the large quadrupole interactions at both centers. We consider the second-order corrections to the hyperfine energies of the $S = {}^1/_2$ ground state. When H_o is along the *x*- or *y*-direction, these arise principally from the cross terms between the fine structure (D_1, D_2) terms and secular components of the hyperfine interaction. The effective perturbation Hamiltonian is then (H_o along *x*, for example)

$$H' = D_1 S_{1z}^2 + D_2 S_{2z}^2 + A_{1x} S_{1x} I_{1x} + A_{2x} S_{2x} I_{2x} + \text{nonsecular terms} \quad \text{(A9)}$$

The nonsecular hyperfine (A_y, A_z, etc.) and quadrupole terms contribute negligible or zero effects at X-band to the second-order corrections.

The first-order (high-field) solutions, analogous to eq A1 above, are (including nuclear basis functions, $|\mu_1\rangle$, $|\mu_2\rangle$)

$$|i\rangle_l^u = |_l^u\rangle[\sum_{(\mu_1,\mu_2)} a(i)_{\mu_1\mu_2}|\mu_1\rangle|\mu_2\rangle] \quad \text{(A10)}$$

$$|_l^u\rangle = \frac{1}{\sqrt{2}}\left[\left|\frac{1}{2}\frac{1}{2}\right\rangle \pm \left|\frac{1}{2} -\frac{1}{2}\right\rangle\right] \qquad \mu_1,\mu_2 = -\frac{5}{2} \cdots + \frac{5}{2}$$

i labels one of the 36 possible nuclear hyperfine states for electron spin up (or down), as would be obtained from the numerical solution of the multiline Hamiltonian, as in ref 18. The *a*'s are the coefficients for the nuclear spin basis functions, assumed here for simplicity to be quantized along *x*. Their explicit forms are not required. The S_{1x}, S_{2x} terms in eq A9, being rank 1 tensor operators, couple the $S = {}^1/_2$ state only to the $S' = S \pm 1 = {}^3/_2$ state.

Because of the substantial nuclear state "mixing" caused by the quadrupole terms, the $a(i)_{\mu_1\mu_2}$ values for a given hyperfine state are nonzero over a range of μ_1,μ_2 values. In addition, and as a consequence, transitions between states $|i\rangle^u$ and $|i'\rangle^l$ ($i \neq i'$) become partially allowed. Thus, for any given orientation of the molecular axis, many more (typically hundreds) than the 36 nominally allowed transitions have significant intensity. Each "line" in the resulting powder pattern spectrum contains many transitions within its envelope. This means that the second-order effects, as long as they are not large, are best regarded statistically.

For a particular nuclear state, *i*, the second-order analysis gives for the energy corrections, ΔE:

$$\Delta E = \frac{2}{15|J|}[7D_1 + 2D_2][A_1(i) - A_2(i)] \quad \text{(A11)}$$

where

$$A_1(i) = \sum_{(\mu_1,\mu_2)} |a(i)_{\mu_1\mu_2}|^2 \mu_1 A_1 = \langle\mu_1\rangle_i A_1, \text{ etc.} \quad \text{(A12)}$$

$\langle\mu_1\rangle_i$ is an average value of μ_1 for the state *i*. Now, $A_{1x,y} \approx 2A_{\perp av}$ and $A_{2x,y} \approx -A_{\perp av}$, where $A_{\perp av} \approx -10$ mT is an average true single-ion $A_\perp$ value for the Mn centers in the multiline dimer. From our earlier multiline simulations, $-(2\langle\mu_1\rangle + \langle\mu_2\rangle) \approx 2-3$ for most of the downfield peaks, particularly toward the pattern edge (opposite sign upfield). Hence, eq 12 follows. This statistical "blurring" of the energy levels probably contributes to the apparently greater line broadening and loss of hyperfine detail seen in alcohol-free samples.

JA981471C